ELSEVIER

Spatial Scaling of a Remotely Sensed Surface Parameter by Contexture

*Jing M. Chen**

Various remote sensing sensors observe the Earth's surface at different spatial resolutions. In deriving surface parameters using remotely sensed data, the transportability of algorithms from one resolution to another is often of great concern because of the surface heterogeneity. This article addresses this scaling issue through image degradation experiments using a Landsat TM image. It is shown theoretically that scaling problems in deriving surface parameters exist not only because of the nonlinearity in the relationships between remote sensing measurements such as NDVI (normalized difference vegetation index) and SR (simple ratio) and the parameters of interest, but also because of the discontinuity between contrasting cover types within a mixed pixel. To quantify the effects of the nonlinearity and discontinuity on scaling, it is found that contextural parameters are more effective than textural parameters. Contexture-based functions are derived for the estimation of the scaling effects on leaf area index (LAI) calculations using algorithms based on NDVI and SR separately. Based on NDVI–LAI and SR–LAI relationships that were derived at the Landsat TM scale (30 m) as part of the Boreal Ecosystem–Atmosphere Study (BOREAS), the effects of scaling on the retrieval of LAI were investigated using nine selected areas of the same size (990 m×990 m) but different water area fractions. The following conclusions are drawn from the investigation: 1) Negative biases in the estimation of LAI occur when either the NDVI or SR algorithm derived at a fine resolution (Landsat TM) is used for calculations at a coarse resolution (for example, AVHRR). 2) The amount of the biases depends on the surface heterogeneity. For a pure forest pixel, the bias caused by the nonlinearity of the NDVI algorithm was smaller than 2% and the linear SR algorithm induces no error in scaling. Therefore, the scaling problem for pure pixels may be ignored for many applications using either linear or nonlinear algorithms. 3) Large negative biases occur when a pixel contains interfaces between two or more contrasting surfaces. In the case of two contrasting surfaces between vegetation and open water, the biases can be up to 45% of the correct value depending of the water area fraction in the pixel. The biases in this case depend on contexture and little on texture. Simulations show that the most useful contextural parameter for quantifying the scaling effects in vegetation–water mixed pixels is the water area fraction within each degraded pixel. Algorithms for remote sensing applications can be transported from one scale to another, if the information on the water body size is available. This study shows the need for global water masks at high resolutions for the purpose of accurate derivation of surface parameters maps at various resolutions. In boreal regions, this is particularly important because of the large number of small water bodies.

INTRODUCTION

With the advent of the forthcoming Earth Observation System (EOS) and other satellite systems, planet Earth will soon be closely watched by multiple sensors with various observing geometries, and spatial and temporal resolutions. In quantitative analysis of remote sensing, the relationship between the measurements at different spatial resolutions often causes concerns. Intrinsic to the measurement techniques, remote sensing is a process of acquiring the average radiative signals from elemental grid cells (pixels) of an object of interest (Townshend, 1980). This signal-averaging process masks subpixel variations and the averaged signals at different resolutions can induce biases when used to retrieve quantitative information. This is often referred to as the spatial scaling effect and has importance in ecological studies (Ehler-

* Applications Division, Canada Centre for Remote Sensing, Ottawa, Ontario, Canada

Address correspondence to Applications Division, Canada Ctr. for Remote Sensing, 419-588 Booth St., Ottawa, Ontario, Canada K1A 0Y7. E-mail: chen@ccrs.nrcan.gc.ca

Received 16 May 1997; revised 2 November 1998.

655 Avenue of the Americas, New York, NY 10010

0034-4257/99/$–see front matter
PII S0034-4257(99)00006-1

inger and Field, 1993). The meanings of spatial scaling in remote sensing of the Earth's surface are several, and are related to how remote sensing data are used. They may be summarized as follows: 1) As an estimate of the average conditions for an area based on the knowledge for the conditions of each scene component and the area fractions of the components in a remote sensing scene. Scaling in this case is an area-weighting operation. 2) For use of remote sensing measurements at various resolutions for deriving surface parameters (such as LAI). Scaling in this case requires the knowledge of surface heterogeneity and depends on the derivation algorithms. 3) For using remotely derived parameters as surrogates for estimating processes, such as gas and energy exchanges between the surface and the atmosphere. Scaling in this case not only depends on the surface heterogeneity, but also the correlation between surface and atmospheric variables involved in the processes (Hall et al., 1992). These three scaling operations mentioned in sequence have increasing complexity, and the methodologies are still far from maturity, especially the second and third scaling problems (Bonan et al., 1993). The last problem is of particular concern to climate-related research (Pielke et al., 1991; Wood and Lakshmi, 1993). In this article, we will focus on the second problem because it is a key step in remote sensing applications, and the principles found in this step have implications to more sophisticated scaling problems.

It has been demonstrated in various ways that linear algorithms cause no error in deriving surface parameters over heterogeneous surfaces (Hall et al., 1992; Hu and Islam, 1997). In selecting optimum resolutions for remote sensing applications and estimating the scaling effects on surface parameter derivation, surface heterogeneity has been exclusively quantified using statistical measures related to the image texture, such as variance and covariance (Woodcock and Strahler, 1987; Hall et al., 1992), and entropy (Townshend and Justice, 1988). The apparent conclusions for the absolute superiority of linear algorithms and the effectiveness of texture-based methodologies are challenged in this article. For the purpose of developing a simple and effective methodology for estimating the scaling effects on the derivation of surface parameters, this article is intended to show through theoretical developments and sample image analysis that: 1) Discontinuity as part of the surface heterogeneity is the major problem in scaling and the linearity of algorithms does not alleviate the problem; and 2) contextural parameters are far more effective than textural parameters in quantifying scaling effects.

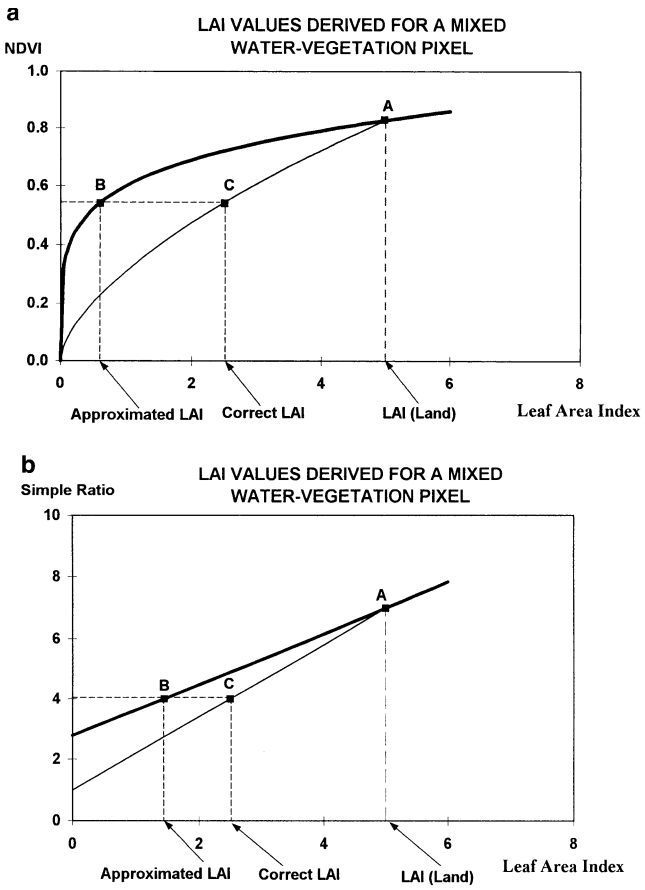

Figure 1. Relationships between NDVI and LAI (a) and between SR and LAI (b) found by Chen and Cihlar (1996) for boreal conifer forests. When the relationships are used for an equally mixed water–land pixel, the intercept *A* represents the LAI value over the land portion (LAI_{land}) and the intercept *C* gives the correct average LAI value for the pixel. The intercept *B* is obtained using the average NDVI value for the pixel and the relationships. The difference between *C* and *B* is the scaling error (see also the Appendix).

THEORY

Problems Due to Nonlinearity and Discontinuity

To aid the theoretical development, we first provide Figures 1a and 1b as examples showing relationships between the normalized difference vegetation index (NDVI) and LAI and between the simple ratio (SR) and LAI reported by Chen and Cihlar (1996) for boreal conifer forests. The nonlinear relationship between NDVI and LAI rather than their linear relationship is chosen for exploration in this study. Models and measurements show that the relationship is nonlinear (Huete and Liu, 1994). Over a pure land surface, the curve should start from a positive NDVI value representing the background. The curve is forced through the origin in this case so that the equation becomes general for application across the landscape, including open water bodies. The linear SR–LAI relationship generally has larger correlation coefficients than the nonlinear NDVI–LAI relationship (Chen, 1996). In this article, the scaling effects of linear and nonlinear algorithms are studied based on these two relationships. In Figure 1a, a simple case is presented where a pixel is composed of half water (NDVI=0 and LAI=0) and half vegetation (NDVI=0.8 and LAI=5). By definition, the

LAI value for the pixel is 2.5. However, from the mean NDVI value of 0.54 obtained using pixel-averaged reflectances (see the Appendix), an LAI value of 0.6 is found using the nonlinear relationship for pure land surfaces. In Figure 1b, a similar problem exists for the linear relationship because of the discontinuity at LAI=0: SR is often larger than 1 for the bare land surface but equal to or smaller than 1 for water bodies. For simplicity, we take SR=1 for water, corresponding to NDVI=0 for water. For clear and deep waters, NIR reflectance is smaller than red reflectance, and hence SR is smaller than 1. For shallow or turbid waters, SR can be larger than 1. The linear relationship would incur no error between different resolutions over pure land surfaces, but can still be a problem when interfaces between contrasting cover types exist in the same pixel.

Mathematically, the correct way to obtain LAI for a large pixel (for example, AVHRR 1 km pixel), denoted by $(\overline{L})$, consisting of n small pixels (for example, Landsat TM 30 m pixels), is to calculate the LAI value of each small pixel, denoted by L_i, and then take the arithmetic mean of all of the small pixels, that is,

$$\overline{L}=\frac{1}{n}\sum_{i=1}^{n} L_i. \tag{1}$$

The LAI of the small pixels should be calculated at the same spatial resolution at which the particular algorithm for L_i was developed.

If the algorithm is represented by Eq. (2),

$$L_i=f_s(VI_i), \tag{2}$$

for the small pixels, where VI_i is a vegetation index for pixel i, Eq. (1) can be written as

$$\overline{L}=\frac{1}{n}\sum_{i=1}^{n} f_s(VI_i). \tag{3}$$

If only measurements of the large pixels, that is, $\overline{VI}$ are available and the algorithm $f_L(\overline{VI})$ for the large pixels is unknown, the approximate values of LAI of the large pixels can be calculated using the algorithm developed for the small pixels as follows:

$$\overline{L}\simeq f_s(\overline{VI}). \tag{4}$$

When the algorithm $f_s(VI)$ is not linear, such as in Eq. (5),

$$f_s(VI_i)=aVI_i^b, \tag{5}$$

it is obvious that [Eq. (6)]

$$f_s(\overline{VI})\neq\frac{1}{n}\sum_{i=1}^{n} f(VI_i). \tag{6}$$

For example, in the case of one large pixel containing two small pixels, it is true that [Eq. (7)]

$$a\left(\frac{VI_1+VI_2}{2}\right)^b\neq\frac{aVI_1^b+aVI_2^b}{2}. \tag{7}$$

In general [Eq. (8)],

$$\left(\frac{1}{n}\sum_{i=1}^{n} VI_i\right)^b\neq\frac{1}{n}\sum_{i=1}^{n} VI_i^b. \tag{8}$$

This means that because of the nonlinearity of the algorithm, different results are obtained depending on whether the individual bands or VIs are averaged first before the algorithm is applied (in the case where only large pixel measurements are available) or whether the algorithm is applied to the small pixels first, and the results are then averaged (in the case where small pixel measurements are available). In remote sensing applications, very often we are confronted with the first situation: large pixel measurements and small pixel algorithms are available, that is, we are forced to incorrectly average the VIs first and then do the information retrieval. The real question is, therefore, how much are we in error in doing so and how can we correct for the error?

In the case of a linear algorithm (Fig. 1b), a similar problem exists because of the discontinuity of the relationships for different cover types. The extreme case would be a pixel mixed with water and land covered by vegetation, where VI=a_0 and LAI=0 for water and LAI=$a+b$VI for land, where $a_0\neq a$. Therefore, the discontinuity exists at LAI=0. In mathematical expression, the LAI for a mixed pixel with n cover types becomes

$$\overline{L}=c_1(a_1+d_1\,\overline{VI}_1)+c_2(a_2+d_2\,\overline{VI}_2)+\cdots +c_n(a_n+d_n\,\overline{VI}_n) \tag{9}$$

where c_i (i=1, 2, . . . , n) is the fraction of cover type i in the pixel, a_i and d_i are the coefficients of the algorithm for cover type i, and $\overline{VI}_i$ is the average VI value of the cover type i. Equation (9) indicates that the correct calculation of LAI for the mixed pixel requires the knowledge of the fractions of the cover types in the pixel. When only large pixel measurements are given, such knowledge is not available. Usually, the mixed pixel is labeled by the dominant class and only one algorithm for the dominant cover type is used, that is,

$$\overline{L}\simeq a_i+d_i\,\overline{VI} \tag{10}$$

An error is introduced in the calculation using Eq. (10) because other cover types are ignored in the calculation. For example, if a pixel mixed with water and conifer forest is classified as conifer, where a_i and d_i in Eq. (10) are taken as the coefficients for conifer and $\overline{VI}$ is the average VI over the whole pixel (the only value available), is considerable different from the correct equation (9), which can be written for this case as

$$\overline{L}=0+c_i(a_i+d_i\,\overline{VI}_i) \tag{11}$$

where $\overline{VI}_i$ is the average VI over the conifer cover type. The differences between these two equations are: 1) The fraction of conifer in the pixel is considered in Eq. (11) but not in Eq. (10); and 2) VI in Eq. (11) is the average for conifers only, while in Eq. (10) it is for the whole

pixel. The resulting difference in LAI is illustrated in Figure 1b for the case of a pixel with half water and half conifer. This demonstrates that scaling errors can be significant using linear algorithms for mixed pixels.

In spite of this, linear algorithms have the following advantages over nonlinear algorithms in scaling: 1) They incur no errors for pure pixels even if the VI vary greatly within the pixels, while nonlinear algorithms cause errors in proportion to the variance of VI within the pixels; 2) for mixed pixels over land surface, the scaling error using linear algorithms are very small because of the similarity of the algorithms for different cover types; and 3) for the extreme case of mixed water and vegetation pixels, linear algorithms cause smaller errors than nonlinear algorithms, as shown in Figures 1a and 1b.

Quantification of Scaling Effect Using Textural and Contextural Parameters

Texture in an image refers to the variability in tone (brightness) of the pixels (Haralick, 1979). It is often quantified using statistical measures such as range, standard deviation, variance, covariance, skewness, kurtosis, etc. (Irons and Peterson, 1981; Haralick, 1986). Contexture captures the structure and patterns of objects displayed in an image (Mather, 1987). It can be quantified as the number of distinct objects (cover types, for example), the size and shape of the objects, the distance, distribution, and pattern of the objects, the areas and the area ratios of the objects, etc. In studies to quantify the scaling effects to date, textural parameters are often used, and contexture remains unexplored. Similarly to Hall et al. (1992), Hu and Islam (1997) developed a generic framework for formulating "scale-invariant" algorithms for any surrogate parameters using multiple-band digital images based on the textural parameters of the images. The framework, when simplified, can be expressed as Eq. (12):

$$P_D - P_L = f(\textit{variances}, \textit{covariances}), \tag{12}$$

where P_D is the correct value of parameter P for a large pixel calculated from small pixels ("distributed"), P_L is the approximate value of parameter P calculated using the mean measurements from the large pixel ("lumped"), and $f(\textit{variances}, \textit{covariances})$ is a function of variances and covariances of the tones within and among the different bands to quantify the difference between P_D and P_L. Theoretically, variances and covariances are important textural parameters capturing the spatial variability in the surface conditions and, therefore, can be used to estimate the scaling effect. The third- and higher-order terms, such as skewness and kurtosis, can generally be ignored. However, in practice, when only the measurements for the large pixels are made, no subpixel textural statistics are available. Because of this problem, Hu and Islam (1997) developed this "scale invariant scheme" assuming that textural characteristics are scale-independent and, therefore, variances and covariances derived from coarse-resolution images are the same as those from fine-resolution images. It is obvious that scale invariance is an assumption and not a reality. For such an assumption to be valid for a forested area, for example, there needs to be an equal probability of seeing the pure background (soil and moss cover) in high and low resolution images, but, undoubtedly, the probability decreases with increasing pixel size. Another problem with this texture-based approach is that it does not address the issue of mixed pixels discussed in the previous section. When a pixel is mixed with water and vegetation, for example, the variance within the pixel may increase because of the contrast in tone between these two cover types, but the increase has a different meaning compared to the same increase over a pure land surface.

To avoid the above-mentioned problems associated with the limitations using textural parameters, a different scheme for quantifying the scaling effect is proposed here as follows:

$$P_D - P_L = f(\textit{subcomponent fractions}). \tag{13}$$

In Eq. (13), the difference between P_D and P_L is quantified using the fractions of subcomponents (such as cover types) within a pixel. A subcomponent fraction is a contextural parameter. This scheme, when applied to reality, captures the main difficulty that causes scaling problems: surface heterogeneity in terms of cover type change rather than density change within the same cover type. The latter is no problem when a linear algorithm is used [discussed in the previous section and theory in Hall et al. (1992)]. However, the application of this scheme also requires additional subpixel information and has the similar data limitation as the texture-based scheme. In practice, the largest contrast in remote sensing signal is between water and land, and high-resolution water masks are frequently available or can be found by other means. In quantifying the scaling effects, contextural parameters have the following advantages over textural parameters: 1) Contexture is the major cause of variation in remote sensing signals and can be used for scaling more effectively; 2) the contextural parameters, such as the area fraction, is more easily obtained than textural information at high resolutions; and 3) the scaling methodology using contextural parameters is generally simple and can be operationally used in information retrieval from a combination of sensors.

As examples to illustrate the principles discussed above, the function in Eq. (13) is derived in the Appendix for LAI algorithms based on NDVI and SR, separately. In some studies, the effect of scaling from individual bands to NDVI was found to be small and could be ignored, that is, lumped and distributed NDVI could be taken as the same (Hall et al., 1992; Aman et al., 1992), but in others it was shown to be significant (Hu and Islam, 1997). We found that this effect on NDVI is partic-

ularly pronounced when subpixel water bodies exist and developed a simple way to consider it (see the Appendix). The nonlinear NDVI–LAI relationship representing the distributed case for a mixed water–vegetation pixel presented in Figure 1a is derived after considering this effect. After defining the relative difference in LAI ($\Delta L/L$) between the distributed and lumped calculations as $\Delta L/L=(P_D-P_L)/P_{land}$, where P_{land} is the parameter over the land portion of the pixel, we can write from the Appendix that

$$\frac{\Delta L}{L}=(1-w)-(1-w)^{b_0/b} \tag{14}$$

for the NDVI algorithm, where w is the water area fraction in a mixed pixel, b is the exponent in the NDVI–LAI relationship over land, and b_0 is the exponent for a mixed vegetation–water pixel. For the SR algorithm, the function is derived as (see the Appendix)

$$\frac{\Delta L}{L}=\begin{cases}\dfrac{a_1-a_0}{b_1L_{land}}w, & w<\dfrac{b_1L_{land}}{a_1-a_0+b_1L_{land}},\\[2ex] 1-w, & w\geqslant\dfrac{b_1L_{land}}{a_1-a_0+b_1L_{land}},\end{cases} \tag{15}$$

where L_{land} is the average LAI over land within the pixel, and a_0 is the SR value over water.

Using Eqs. (14) and (15), Figures 2a and 2b are plotted to illustrate how the water area fraction w affects the calculation of LAI of a large (lumped) pixel. In Figure 2a, the relative difference in LAI between the distributed and limped calculations based on the NDVI algorithm varies in different magnitudes with w, depending on the constant b. The distribution patterns can be understood by imagining the extreme cases (not plotted): 1) When $b=b_0$, the difference becomes zero at all w values because the NDVI–LAI relationship becomes the same as the distributed function; and 2) when $b=0$, which means NDVI is invariant with LAI, the difference is determined simply by the value of $(1-w)$ (i.e., the diagonal line) and has a maximum at $w=0$. The maximum difference occurs at different w values depending on the value of b. In the Appendix, it is shown to be when $w=1-(b/b_0)^{b/(b_0-b)}$.

Figure 2b shows linear variations of the relative difference in LAI with w when the linear SR algorithm is used. The family of lines result from the additional dependence of the difference on the LAI value over the land portion of the pixel. With the fixed constants in the SR–LAI relationship, the w value at which the maximum difference occurs depends on the LAI value over the land surface. There are similarities between Figures 2a and 2b: 1) The diagonal line sets the upper limit for the difference, and 2) the maximum difference does not occur at a fixed w value, but follows predictable patterns. The major difference between these two algorithms is that in estimating the scaling effect using the NDVI algorithm, the knowledge of LAI over the land surface is not required, but it is needed for the SR algorithm.

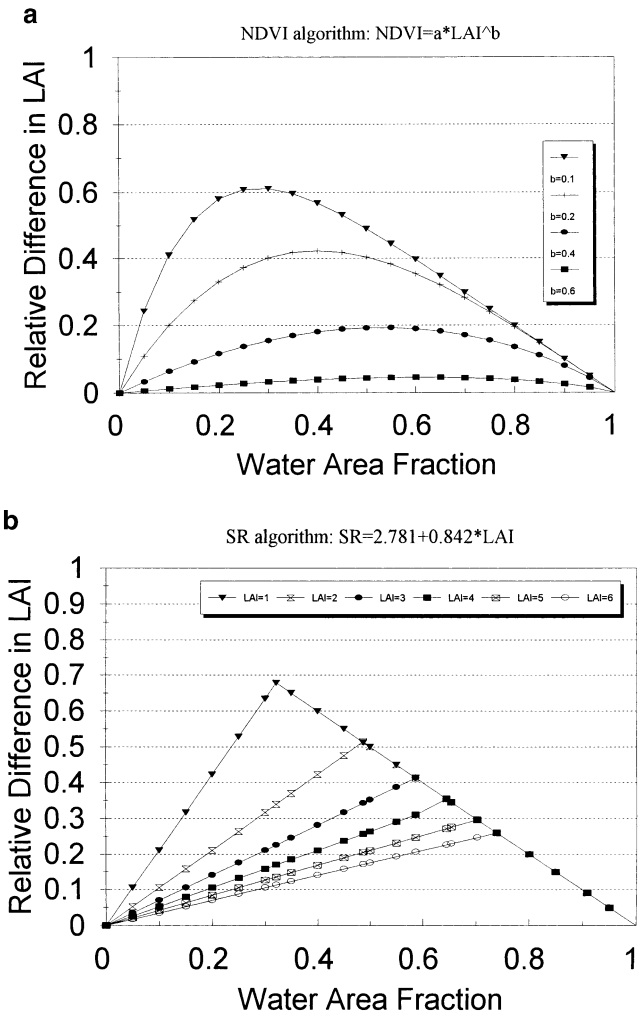

Figure 2. Theoretical relationships between the scaling errors, expressed as the difference in LAI between distributed and lumped calculations relative to the LAI value over land, and the water area fraction within the pixel: a) The relationship depends on the exponent b in the NDVI-LAI algorithm; and b) the relationship is affected by LAI over land within the pixel when the SR algorithm is used.

IMAGES AND ALGORITHMS

A Landsat image is used here to investigate the scaling effect (Fig. 3). The size of the image is 61.44 km×61.44 km, which is part of the original scene (row number 37/22–23) acquired on 6 June 1991 at a solar zenith angle of 35.9°. It is one of the images used by Chen and Cihlar (1996). Candle Lake, Saskatchewan, Canada, is the largest lake located near the southwest corner. A large number of open water bodies are shown in the image and they are the main cause of surface heterogeneity. The image shown in Figure 3 is an NDVI image calculated from the original TM Bands 3 and 4 after atmospheric corrections using the 5S code (Tanré et al., 1986). In Figure 3, nine areas of 990 m×990 m (33×33 pixels) each were selected for their different area frac-

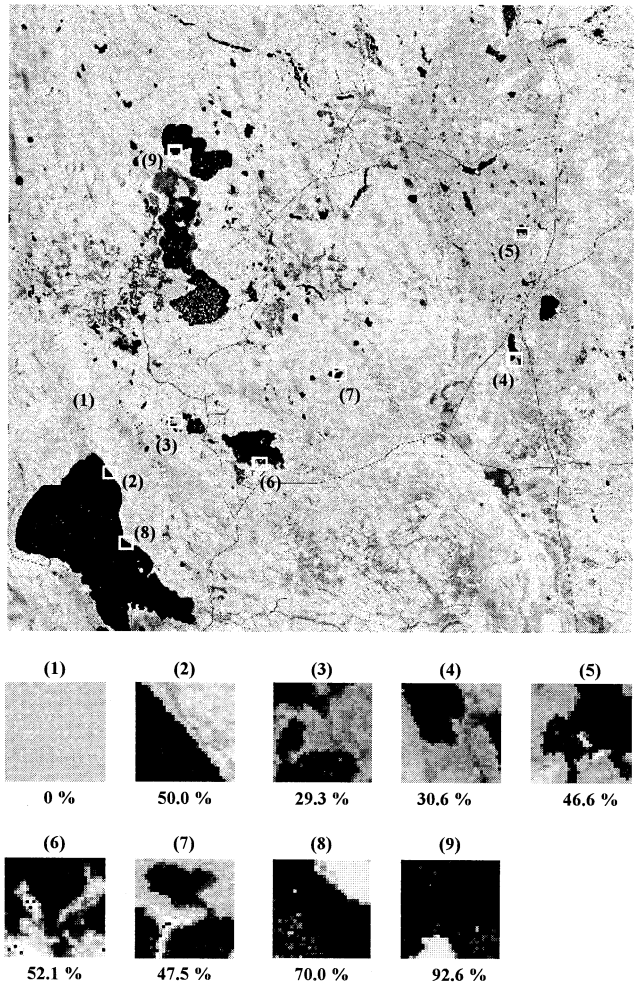

Figure 3. A Landsat NDVI image of size 61.44 km×61.44 km, where nine areas of 990 m×990 m each are selected for scaling analysis.

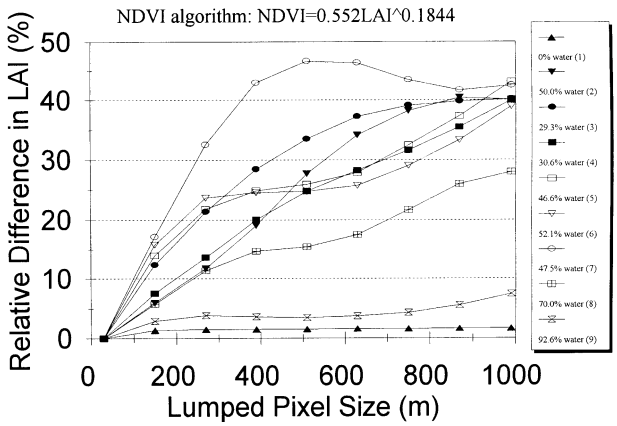

Figure 4. Variations of the NDVI-based scaling error, expressed as the relative difference in LAI for the nine selected areas in Figure 3, as the lumped pixel size increases. The area number is shown in the brackets in the legends.

tions of water ranging from 0% to 93%. The following relationships [Eqs. (16) and (17)] between LAI and NDVI and between LAI and SR for conifers (Chen and Cihlar, 1996) are used in this study:

$$NDVI = 0.552L^{0.1844} \tag{16}$$

and

$$SR = 2.78 + 0.824L. \tag{17}$$

These are the equations derived for late spring. The *R*-squared values for these relationships are 0.52 and 0.53, respectively. These linear and nonlinear relationships are chosen to demonstrate the major scaling problems associated with nonlinearity and discontinuity.

RESULTS AND DISCUSSION

Scaling Effects from Landsat TM to AVHRR Scale

The nine areas marked on the Landsat image (Fig. 3) were selected to investigate scaling methodologies based on contexture. The enlarged nine areas and their w values are also provided in Figure 3. Figure 4 shows the difference in LAI between the distributed [Eq. (3)] and lumped [Eq. (4)] calculations for various lumped pixel sizes using the NDVI algorithm, where NDVI at a given pixel size is obtained from the mean band reflectances. By definition, a positive difference in LAI means the lumped calculation is negatively biased, and this will always be the case. The difference in the LAI values at different scales of image degradation is obtained as the average of many subareas of the same size by shifting the pixel and line one pixel at a time within the original 33×33 pixel frame. At the 30 m scale, both types of calculations were done at the original TM pixels, and therefore no difference in LAI results are found. At the 990-m scale (representing 1 km AVHRR pixels), these two types of calculations result in large differences in calculated LAI values. The magnitude of the difference depends on the water area fraction within the lumped pixels. For area 1 without water, the differences at the various sizes are less than 1.7% of the value calculated using the distributed method, indicating that, over a pure land surface, the error in scaling is very small even when a nonlinear algorithm is used. The curves in Figure 4 vary, in different patterns with image degradation. These patterns will be investigated in the next section. We will first focus on the results at the largest pixel size of 990 m at which the water area fraction is calculated. Figure 5 shows how well the theory [Eq. (14)] predicts the scaling effect found in Figure 4 at the lumped pixel size of 990 m. Although completely different calculations are involved—the data points are obtained from pixel-to-pixel calculations while the curve is calculated using only three parameters (w, b=0.1844, and b_0=0.68)—the agreement is very encouraging, showing the effectiveness of this contexture-based method for estimating the scaling effect.

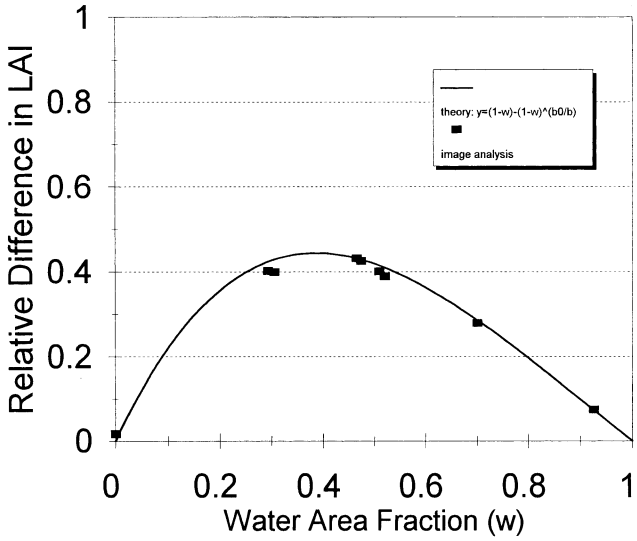

Figure 5. Comparison of the theoretical estimation of the scaling effect with those from image analysis for the nine selected areas at the lumped pixel size of 990 m shown in Figure 4.

For the same nine areas, the scaling effects estimated based on the SR algorithm are shown in Figure 6. The curve variation patterns are similar to those shown in Figure 4, but the magnitude of the scaling effect is often smaller, indicating one advantage of using the linear SR algorithm. Another advantage of the SR over the NDVI algorithm is that the scaling effect is zero over a pure land surface as indicated by the bottom line. This is in agreement with the aforementioned theoretical analysis. The major disadvantage of the SR algorithm for estimating the scaling effects is the requirement of the additional parameter of LAI over the land surface within the pixel. This information is generally not available when

Figure 6. Variations of the SR-based scaling error, expressed as the relative difference in LAI for the nine selected areas in Figure 3, as the lumped pixel size increases. The area number is shown in the brackets in the legends.

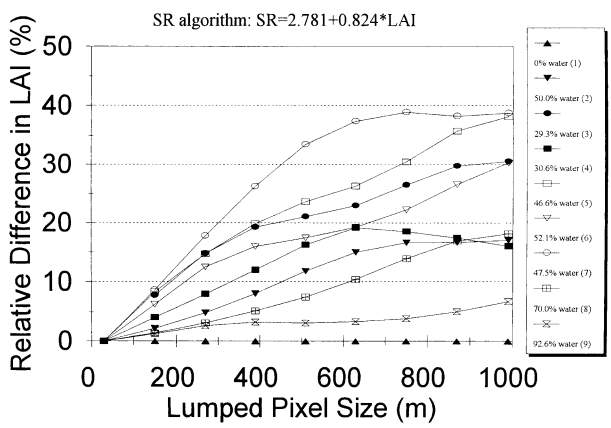

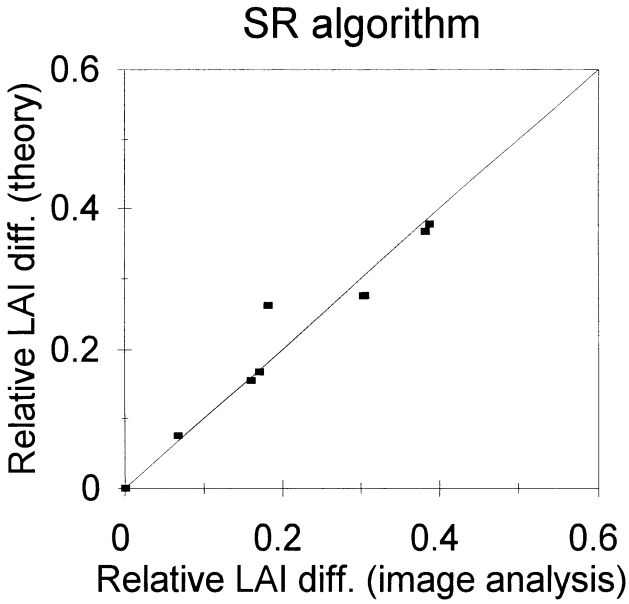

Figure 7. Comparison of the theoretical estimation of the scaling effect with those from image analysis for the nine selected areas at the lumped pixel size of 990 m shown in Figure 6. In the theoretical estimation, both water area fraction and the mean LAI value over land within the areas are used [Eq. (15)].

measurements are derived for large pixels. In practice, this may not be a problem because it can be taken as the value of an adjacent pure land pixel as the first approximation. Figure 7 compares the relative difference in LAI found in Figure 6 at the lumped pixel size of 990 m through image analysis to theoretical predictions using Eq. (15). The LAI value over the land portion was first found for each area. The value is, in order from area 1 to 9 (marked in the legends of Fig. 6), 3.47, 6.36, 1.96, 4.19, 2.45, 2.99, 2.37, 3.63, and 4.05. The theoretical predictions for the scaling effect agree very well with the values obtained from the image analysis, except for one point, which is area 8. As shown in Figure 3, this area contains some shallow water pixels which are considered as land using a common threshold of NDVI=0.2. If these pixels are considered as water, the discrepancy between the theory and image analysis would disappear. This, however, raises a question of how to separate water and land for this type of applications. In areas with shallow waters, more attention should be given to the choice of water-land threshold.

From the above analysis, it is shown that SR algorithms have the following advantages over NDVI algorithms: 1) They incur no scaling errors when applied to a pure pixel with only one cover type regardless of the change in density within the pixel; and 2) they induce smaller scaling errors than NDVI algorithms if no corrections for the errors are made. The estimation of the scaling errors based on SR algorithms, however, are more

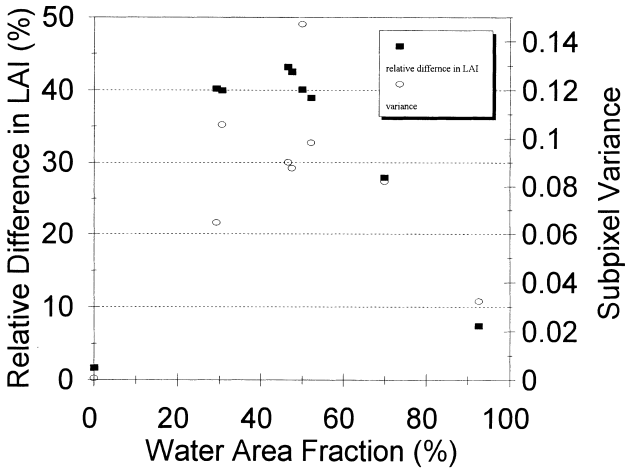

Figure 8. Comparison of the NDVI-based scaling error with the total subpixel variance in NDVI for the nine selected areas of difference water area fractions.

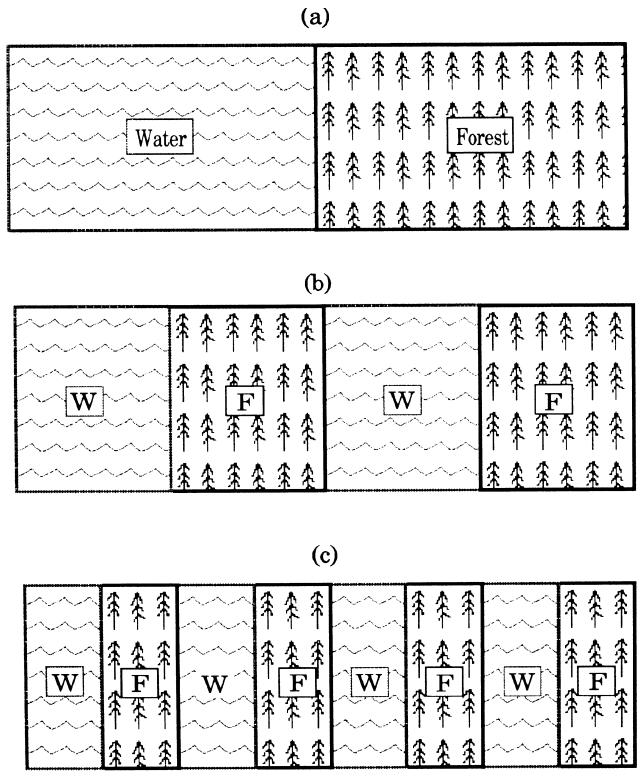

Figure 9. Three one-dimensional (horizontal) cases of a pixel equally mixed with forest and water but having different water body sizes (270 m, 540 m, and 1080 m) within the pixel for numerical simulation of the effect of subpixel water body size on scaling. Variations in the second dimension (vertical in the plates) are not considered.

complicated than that based on the NDVI algorithms. Although the requirement of the LAI value over land surface within a mixed pixel can be obtained from the adjacent pure land pixels, the subpixel variation in LAI still have significant secondary effects on the estimation of scaling errors.

Figure 8 compares the scaling effects using the NDVI algorithm shown in Figure 5 and the values of the total variance as a textural parameter within the selected nine areas. The variance has the largest value at w=50% and falls off on both sides as w increases or decreases from the center value, while exhibiting considerable scatter for the same w values depending on the variation of NDVI over land. This comparison suggests that the textural parameter can provide the first-order approximation for the scaling effect, but the estimate is much less precise than those based on the contextural parameter w as demonstrated in Figure 5.

Effects of Subpixel Component Size

The image analysis results displayed in Figures 4 and 6 have only been partially studied in the above section. The different curve patterns and the crossings of the curves impose questions on the uniqueness and effectiveness of the contextural parameter. To address this issue, numerical simulations were conducted to illustrate the effects of subpixel water body size on scaling from the elemental (30 m) to various lumped pixel sizes. Figure 9 shows imaginary pixels equally mixed with forest and water bodies having different spatial dimensions, that is, different patterns as exhibited in plates (a), (b), and (c). The examples are all one-dimensional for simplicity; only horizontal variations of the forest and water land covers are considered. In numerical simulations, the total horizontal width is taken to be 2160 m for all three cases, and the smallest pixel size is 30 m to represent Landsat TM pixels. The red and NIR reflectances are assigned the values of 0.17 and 0.03, respectively, for forest, and the same at 0.02 for water. Figure 10 shows the effects on LAI of scaling from 30 m to various spatial scales for the three cases. The scaling effects at the various lumped pixel sizes are simulated by performing distributed and lumped calculations using the same NDVI algorithm as used previously on a horizontal line consisting of 720 pixels. A lumped LAI value for a given pixel size is calculated from the mean NDVI value over a section of the line equal to the size, while the paired distributed LAI value is calculated as the mean of LAI values of individual pixels over the same section. The scaling effect is obtained as the average of the relative differences between distributed and lumped LAI values of many sections moving one pixel at a time along the line. Figure 10 demonstrates that, for the same water area fraction in an area or region, the scaling effects for a given spatial resolution are different for different water body sizes within the area (represented by the horizontal width in this case). Larger water bodies generally incur smaller scaling effects for a given pixel size. This subpixel size dependence explains the irregular curve patterns shown in Figure 4 where water bodies included in the

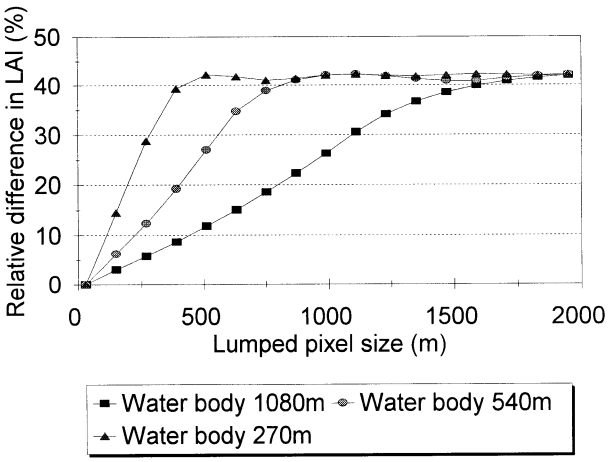

Figure 10. Scaling effects on the relative difference in LAI at the various lumped pixel sizes for the three cases of different water body sizes shown in Figure 9.

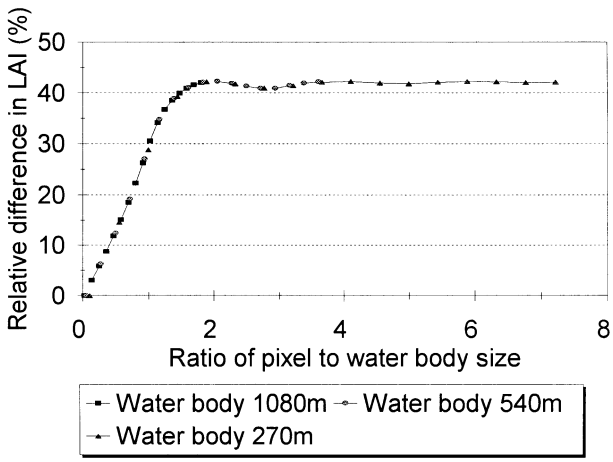

Figure 11. Normalization of the scaling effects shown in Figure 10 using the ratio of lumped pixel to water body size.

calculations have different sizes. Areas 5 and 7, for examples, have similar water area fractions, 46.6% and 47.5%, respectively, but area 5 shows slower increases in the scaling effects with the increasing pixel size because it contains a larger water body than those in area 7. The same reason can be given for difference between the curves for the areas 3 and 4 with similar water area fractions of 29.3% and 30.6%. The water bodies in area 3 is smaller than those in area 4. The curve distribution patterns in Figure 6 are less variable than those in Figure 4 but are also affected by the water body size in a similar way.

A key to understanding Figures 4 and 6 is that the water area fraction specified for each curve is the value for the whole area 990 m×990 m and this value does not necessarily remain the same for the mean value for many smaller lumped pixels within the area. Equations (14) and (15) can be applied to a pixel of any size and only require the water area fraction for the pixel (not an area of multiple pixels) to be given. In other words, the scaling effect shown in Figures 4 and 6 at each lumped pixel size can be predicted with these equations when accurate water area fraction values for all the pixels are available. This means that, in assessing the scaling effect on remote sensing measurements of a given resolution, we only need the water area fraction information for each pixel and do not need the water body size information. The size information is needed only if we want to infer the scaling effect from one resolution to the other. This basic requirement greatly simplified the procedure for estimating the scaling effect when a contextural parameter is used. From a dimensional analysis, the effect of water body size on scaling between various pixel sizes is more effectively quantified using the dimensionless variable: the ratio between the pixel size to the water body size. Figure 11 shows how the scaling effects shown in Figure 10 are normalized to this ratio. It demonstrates that once the NDVI–LAI algorithm is given, the scaling effect for various lumped pixel sizes can be uniquely determined by the ratio. The effectiveness of this normalization implies that when water body size information is available, a complete analysis of scaling effects for images of various resolutions can be easily made.

DISCUSSION

Examples shown in this article are limited to two algorithms and one biophysical parameter. However, the principles of scaling effect estimation using contextural parameters should apply to other parameters (such as the fraction of photosynthetically active radiation observed by vegetation, temperature, etc.) using algorithms based on other vegetation indices. The effectiveness of these contexture-based scaling algorithms has the following implications:

1. Nonlinearity in remote sensing algorithms is not the only problem to be considered in scaling between different resolutions. Differences in the relationship between remote sensing signals and the surface parameter of interest create discontinuities in the mathematical description of the signals from mixed pixels. These discontinuities also induce errors in scaling, and generally errors due to discontinuities are much larger than those due to nonlinearity.
2. From the scaling perspective, the surface heterogeneity should not be viewed to be equivalent to texture variation. When linear algorithms are used, textural variations cause no error in scaling if no interfaces between cover types are encountered in the area. Interfaces within mixed pixels are the major problem in scaling using either lin-

ear or nonlinear algorithms. Therefore, the surface heterogeneity can be more effectively quantified using contextural parameters. The best strategy for minimizing and quantifying the scaling effect is to use linear algorithms and contextural parameters.

3. Contexture-based scaling methodologies may also be useful for estimating the effects of surface heterogeneity on surface–atmosphere mass and energy exchange calculations using remote sensing data. The correlation between variables involved in the exchange processes, which is the main cause of the scaling problem, may also be quantified using contextural rather than textural parameters because the existence of water bodies or mixed cover types in a pixel may be the main reason for the correlation between the variables. For example, partial water coverage in a pixel can cause strong spatial correlation between surface temperature and evapotranspiration. After comprehensive numerical simulations. Bonan et al. (1993) turned to "statistical representation of multiple land surfaces within a grid cell" for mesoscale and climate models. This implies a contextural representations.

CONCLUSIONS

Through theoretical derivation and image analysis, it is demonstrated that a contextural parameter based on the fractions of subcomponent areas is effective for quantifying the scaling effect on deriving surface parameters. In scaling remote sensing measurements over terrestrial surfaces, mixed landcover types in a pixel are the major problem causing scaling errors. The principles of the contexture-based methodology are shown using examples of land–water mixed areas because the interface between land and water has the largest contrast and is of key concerns in scaling. The most important conclusion of this study is that for accurate derivation of surface parameters for images at a given spatial resolution, a water mask at a higher resolution is required. In using AVHRR images, for example, a water mask giving the percentage of open water bodies in each pixel is very useful for improving surface parameter maps. Since a water mask is fairly stable with time (if floods and transient water bodies are excluded), it would be a worthwhile long-term investment to produce such a mask for a given region of interest and for the globe using mosaics of high resolution images such as from Landsat or SPOT.

In addition, the following technical conclusions are drawn:

1. Contexture-based methods for quantifying scaling effects on the derivation of biophysical parameters are not only alternatives to the methods based on textural parameters but also more effective and simpler. The required subpixel contextural information is also easier to obtain than textural parameters.
2. Linear algorithms such as those based on SR have an advantage of error-free scaling over surfaces with density changes without interfaces between cover types. However, linear algorithms also induce scaling errors for mixed pixels because of the interfaces. Mathematically, the interfaces cause discontinuities in the algorithm and these discrete changes in the surface properties are better quantified using contextural rather than textural parameters.
3. Nonlinear algorithms, such as those based on NDVI, have both problems of nonlinearity and discontinuity. The nonlinearity causes scaling errors even for surfaces with only density changes, but the errors are generally very small (a few percent). The discontinuity problems are similar to those of SR-based algorithms and not investigated here.
4. For the most common scaling problem across land-water interfaces, the nonlinear algorithm based on NDVI when forced through the origin (i.e., NDVI=0 at LAI=0) induces no discontinuity problem, and the methodology for estimating the scaling effect is simpler than that based on SR with a discontinuity problem. In using such an NDVI algorithm, only the information of the water area fraction within a pixel is needed for accurate estimation of the scaling effect. When a SR algorithm is used, an additional input for the parameter value over land within the mixed pixel is required. This would induce a small uncertainty, although the value can be readily estimated from the neighboring pure land pixels.

The author is indebted to Dr. Josef Cihlar for helpful discussions. The assistance of Micheal Sarich and Eddy Yu is greatly appreciated. Gunar Fedoseyevs provided useful comments on an early version of this manuscript.

APPENDIX: SCALING BASED ON CONTEXTURE

Scaling from Bands to Vegetation Indices

A specific case of a mixed vegetation–water pixel is demonstrated here. With the water area fraction of w in the pixel, the mean pixel reflectances in the red and NIR channels are given in Eqs. (A1) and (A2):

$$\rho_r = w\rho_{rw} + (1-w)\rho_{rl} \tag{A1}$$

and

$$\rho_n = w\rho_{nw} + (1-w)\rho_{nl}, \tag{A2}$$

where ρ_{rw} and ρ_{rl} are the red reflectance of water and land surfaces, respectively, and ρ_{nw} and ρ_{nl} are the near-infrared reflectance of water and land surfaces, respectively. The mean NDVI and SR for the pixel from these mean pixel reflectances are

$$NDVI=\frac{w(\rho_{nw}-\rho_{rw})+(1-w)(\rho_{nl}-\rho_{rl})}{w(\rho_{nw}+\rho_{rw})+(1-w)(\rho_{nl}+\rho_{rl})} \quad \text{(A3)}$$

and

$$SR=\frac{w\rho_{nw}+(1-w)\rho_{nl}}{w\rho_{rw}+(1-w)\rho_{rl}}. \quad \text{(A4)}$$

Equations (A3) and (A4) can be considered as the first step in scaling: from bands to vegetation indices (VIs). This step is important because remote sensing measurements are obtained as the means of individual bands at a given resolution, and VIs calculated from the mean reflectances of the individual bands are different from those calculated as the means of VIs of small pixels.

Figure 12a shows how NDVI and SR change with subpixel w theoretically, where $\rho_{rl}=0.03$, $\rho_{nl}=0.17$, and $\rho_{rw}=\rho_{nw}=0.02$. These values are representative values for the boreal landscape. For clear and deep waters, $\rho_{rw}>\rho_{nw}$, but they are taken as the same here for simplicity since the absolute difference (after atmospheric correction) is small. The NDVI–w relationship is strongly nonlinear, indicating that the scaling from individual channels to NDVI is a necessary step. The SR–w relationship is approximately linear, suggesting that SR has an advantage over NDVI in this initial scaling step. Figure 12b shows the similar relationships found from the nine selected areas (Fig. 3). It is shown that the linear SR–w relationship is appropriate, and that NDVI is indeed nonlinearly related to w. For the mathematical convenience of deriving the NDVI–LAI scaling algorithm below, this NDVI–w relationship is approximated using the power function. As shown in Figure 12b, the power function captures the nonlinearity reasonably well, but may cause some error at low w values. These linear and power relationships are then used in SR and NDVI scaling algorithms in this study.

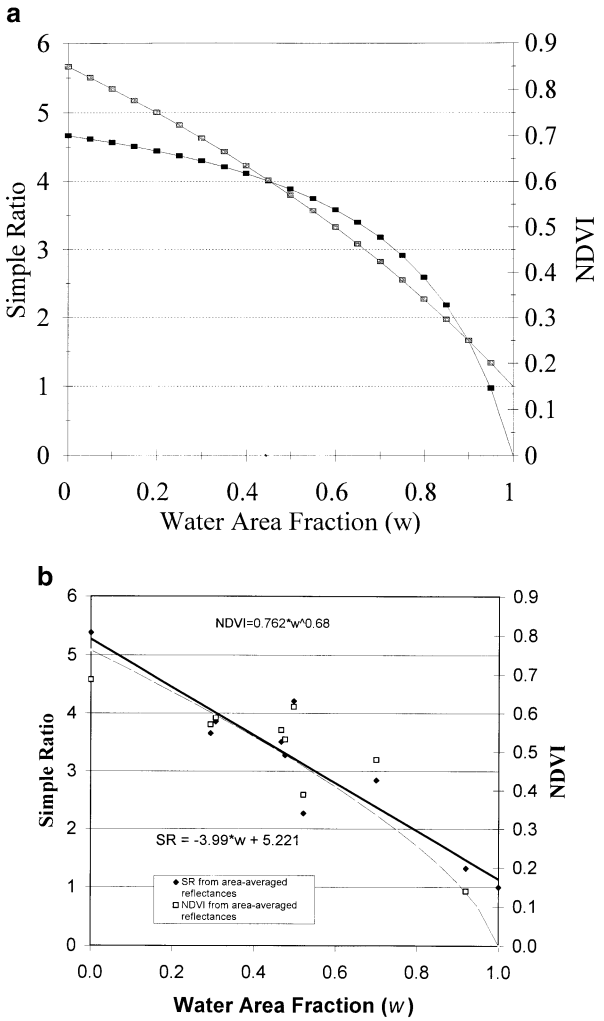

Figure 12. Variation of NDVI and SR with subpixel water area fraction: a) theory [Eqs. (20) and (21)]; (b) data from the nine selected areas (Fig. 3).

NDVI Algorithm

The schematic diagram shown in Figure 1a is referred to here for the calculation of the scaling effect using water area fractions (w) as a contextural parameter. For a pixel consisting of land and water surfaces, the diagram illustrates how the difference in LAI occurs between the distributed and lumped calculations. The relationship between LAI and NDVI for the lumped case (solid thick curve) is

$$NDVI=cL^b, \quad \text{(A5)}$$

where a and b are constants. This relationship is obtained at a fine resolution, but used for a coarse resolution image as a common case encountered in scaling remote sensing measurements. The solid thin curve from the origin represents the distributed NDVI–LAI relationship when the LAI of the land surface has a fixed value of L_{land} and the water area fraction varies from zero (at the intercept A) to 100% (at the origin) assuming NDVI of the water surface is zero. Since LAI in this mixed pixel is proportional to $(1-w)$, this relationship can be described by (Fig. 12b)

$$NDVI=c_0L^{b0}. \quad \text{(A6)}$$

This relationship represents the distributed case because it allows the retrieval of the correct LAI values using the knowledge of w which is to be obtained from small pixels (distributed).

At the intercept A, $c_0L_{land}^{b0}=cL_{land}^{b}$; therefore,

$$\frac{c_0}{c}=L_{land}^{b-b0} \quad \text{(A7)}$$

The difference between the distributed and lumped LAI

estimations is the difference between the intercept points B and C on these two curves by a horizontal line defined by the mean NDVI of the mixed pixel. At C, the LAI value is

$$L_C=(1-w)L_{land}, \tag{A8}$$

and, from Eq. (A6), the NDVI value is

$$NDVI_C=c_0[(1-w)L_{land}]^{b_0}. \tag{A9}$$

Since $NDVI_C=NDVI_B$, from Eq. (A5) we have

$$L_B=\left(\frac{c_0}{c}\right)^{b}[(1-w)L_{land}]^{b_0/b} \tag{A10}$$

From Eqs. (A7)–(A10), the difference in LAI between C and B relative to L_{land} can then be determined as

$$\frac{L_C-L_B}{L_{land}}=(1-w)-(1-w)^{b_0/b}. \tag{A11}$$

Equation (A11) shows that the relative difference between the lumped and distributed calculations is a sole function of w. The exponents b and b_0 in the original nonlinear lumped and distributed relationships have effects on the difference while the constants c and c_0 are eliminated in the derivation. From the derivative of Eq. (A11) with respect to w, it can be found that the maximum difference occurs at $w=1-(b/b_0)^{b/(b_0-b)}$ For the b value of 0.1844 found by Chen and Cihlar (1996) and b_0 value of 0.68 (Fig. 12b), the maximum difference is at $w=0.384$, that is, a pixel containing 38.4% of water surface has the largest effect on the LAI calculation.

SR Algorithm

Figure 1b shows a schematic diagram for estimating the scaling effect using a SR algorithm. It is analogous to Figure 1a, but the NDVI curves are replaced by the SR lines. The lumped case is given by Eq. (A12):

$$SR=a_1+d_1L, \tag{A12}$$

where a_1 and d_1 are constants. Again, this is supposedly an algorithm found at a fine resolution and used for a coarse resolution image. The other line from the intercept a_0 to the point A is defined by Eq. (A13):

$$SR=a_0+d_0L, \tag{A13}$$

where a_0 and d_0 are constants. According to Figure 12, $a_0=1$. The constant d_0 is found from

$$d_0=\frac{a_1-a_0+d_1L_{land}}{L_{land}}. \tag{A14}$$

The LAI value of the C point is then determined in the same way as Eq. (A8). For the B point, it is given as

$$L_B=\begin{cases}\dfrac{SR_B-a_1}{d_1}, & SR>a_1,\ i.e.,\ w<\dfrac{d_1L_{land}}{a_1-a_0+d_1L_{land}}\\ 0, & SR\leqslant a_1,\ i.e.,\ w\geqslant\dfrac{d_1L_{land}}{a_1-a_0+d_1L_{land}}\end{cases} \tag{A15}$$

where $SR_B=SR_c$ and

$$SR_C=a_0+d_0(1-w)L_{land} \tag{A16}$$

From Eqs. (A8) and (A14)–(A16), it can be shown that

$$\frac{L_C-L_B}{L_{land}}=\begin{cases}w\dfrac{a_1-a_0}{d_1L_{land}}, & w<\dfrac{d_1L_{land}}{a_1-a_0+d_1L_{land}}\\ 1-w, & w\geqslant\dfrac{d_1L_{land}}{a_1-a_0+d_1L_{land}}\end{cases} \tag{A17}$$

Equation (A17) shows that the relative difference in LAI between the lumped and distributed calculations using an SR algorithm is a function of both water area fraction and LAI over land, and that the method is slightly more complicated than that using an NDVI algorithm.

REFERENCES

Aman, A., Randriamanantena, H. P., Podaire, A., and Froutin, R. (1992), Upscale integration of normalized difference vegetation index: the problem of spatial heterogeneity. *IEEE Trans. Geosci. Remote Sens.* 30:326–338.

Bonan, G. B., Pollard, D., and Thompson, S. L. (1993), Influence of subgrid-scale heterogeneity in leaf area index, stomatal resistance and soil moisture on grid-scale land–atmosphere interactions. *J. Clim.* 6:1882–1897.

Chen, J. M. (1996), Evaluation of vegetation indices and a Modified Simple Ratio for boreal applications. *Can. J. Remote Sens.* 22:229–242.

Chen, J. M., and Cihlar, J. (1996), Retrieving leaf area index of boreal forests using Landsat TM images. *Remote Sens. Environ.* 55:153–162.

Ehleringer, J. R., and Field, C. B. (1993), *Scaling Physiological Processes: Leaf to Globe*, Academic, Boston.

Hall, F. G., Huemmrich, K. F., Goetz, S. J., Sellers, P. J., and Nickeson, J. E. (1992), Satellite remote sensing of surface energy balance: success, failures, and unresolved issues in FIFE. *J. Geophys. Res.* 97(D17):19,061–19,089.

Haralick, R. M. (1979), Statistical and structural approaches to texture. In *Proceedings of the IEEE*, IEEE, New York, Vol. 67, pp. 786–804.

Haralick, R. M. (1986), Statistical image texture analysis. In *Handbook of Pattern Recognition and Image Processing* (T. Y. Yong and K. S. Fu, Eds.), Academic, New York, pp. 247–280.

Hu, Z., and Islam, S. (1997), A framework for analyzing and designing scale invariant remote sensing algorithms. *IEEE Trans. Geosci. Remote Sens.* 35:747–755.

Huete, A. R., and Liu, H. Q. (1994), An error and Sensitivity analysis of the atmospheric- and soul-correcting variants of the NDVI for the MODIS-EOS. *IEEE Trans. Geosci. Remote Sens.* 32:897–905.

Irons, J. R., and Peterson, G. W. (1981). Texture transforms of remote sensing data. *Remote Sens. Environ.* 11:359–370.

Mather, P. M. (1987), *Computer Processing of Remotely Sensed Images*, Wiley, New York.

Pielke, R. A., Dalu, G. A., Snook, J. S., Lee, T. J., and Kittel, T. G. F. (1991), Nonlinear influence of mesoscale land use on weather and climate. *J. Clim.* 4:1053–1069.

Tanré, D., Deroo, C., Duhaut, P., et al. (1986), *Simulation of the Satellite Signal in the Solar Spectrum*, Laboratoire d'optique atmosphérique, Université des Sciences et Techniques de Lille, 59655 Villeneuve d'Ascq Cedex, France, 343 pp.

Townshend, J. R. C. (1980), The spatial resolving power of earth resources satellites: a review, NASA Goddard Space Flight Center TM 82020, Greenbelt, MD.

Townshend, J. R. G., and Justice, C. O. (1988), Selecting the spatial resolution of satellite sensors required for global monitoring of land transformations. *Int. J. Remote Sens.* 9:187–236.

Wood, E. F., and Lakshmi, V. (1993), Scaling water and energy fluxes in climate systems: three land–atmospheric modeling experiments. *J. Clim.* 6:439–857.

Woodcock, C. E., and Strahler, A. H. (1987), The factor of scale in remote sensing. *Remote Sens. Environ.* 21:311–332.